J Clust Sci (2015) 26:389–409
DOI 10.1007/s10876-014-0829-7

ORIGINAL PAPER

Low-Energy Structures of Binary Pt–Sn Clusters from Global Search Using Genetic Algorithm and Density Functional Theory

Xiaoming Huang · Yan Su · Linwei Sai · Jijun Zhao · Vijay Kumar

Received: 7 August 2014 / Published online: 28 December 2014

Abstract The low-energy structures of Pt_nSn_n (n = 1–10) and $Pt_{3m}Sn_m$ (m = 1–5) clusters have been determined using genetic algorithm incorporated with density functional theory. Platinum and tin atoms tend to mix with each other due to the energetically favorable Pt–Sn bonds. However, due to the larger atomic radius of Sn atoms, we find segregation of Sn atoms on the surface of Pt_nSn_n clusters. This leaves one or two Pt atoms available for reaction and for larger clusters segregation of Sn could block the Pt sites. For $Pt_{3m}Sn_m$ clusters, Sn atoms are well separated in the cluster structures and prefer to form sharp vertices leaving triangular faces of three Pt atoms available for reactivity. The electronic properties such as highest occupied molecular orbital–lowest unoccupied molecular orbital gap, distribution of frontier orbitals, Mayer bond order, Mülliken atomic charge, and the density of

Electronic supplementary material The online version of this article (doi:10.1007/s10876-014-0829-7) contains supplementary material, which is available to authorized users.

X. Huang · Y. Su · J. Zhao (✉)
Key Laboratory of Materials Modification by Laser, Ion and Electron Beams, Dalian University of Technology, Ministry of Education, Dalian 116024, China
e-mail: zhaojj@dlut.edu.cn

X. Huang · Y. Su · J. Zhao
College of Advanced Science and Technology, Dalian University of Technology, Dalian 116024, China

L. Sai
Department of Mathematics and Physics, Hohai University, Changzhou 213022, China

V. Kumar (✉)
Dr. Vijay Kumar Foundation, 1969 Sector 4, Gurgaon 122001, Haryana, India
e-mail: kumar@vkf.in

V. Kumar
School of Natural Sciences, Center for Informatics, Shiv Nadar University, Chithera, Gautam Budh Nagar 203 207, U. P., India

states are discussed. Significant hybridization between the *d* orbitals of Pt and the *p* orbitals of Sn is revealed. These theoretical results provide the general trends for the structural and bonding characteristics of the Pt–Sn alloy clusters and help understand their catalytic behavior.

Keywords Low-energy structures · Genetic algorithm · Density functional theory

Introduction

Platinum is an important catalyst for a variety of reactions, such as dehydrogenation of paraffin [1], oxidation reaction or oxygen reduction reaction and electro-oxidation [2]. In realistic applications such as CO oxygenation, Pt catalysts can be easily poisoned due to blocking of active sites by carbon and the activity is thus degraded quickly, which is an urgent issue to be solved.

Compared to the elementary transition metals, binary alloys have an advantage as catalysts because the geometries and electronic properties of their clusters and nanoparticles can be manipulated additionally by changing composition. Platinum based binary alloys such as Pt–Co, [3, 4] Pt–Ni, [3] Pt–Pd, [5] Pt–Ru, [6–9] and Pt–Sn [8, 10–18] have been widely investigated experimentally. Among them, Pt–Sn alloys are particularly attractive owing to their excellent performance as catalyst. Recently, Antolini and Gonzalez [15] summarized the electronic catalytic activity of Pt–Sn catalysts for methanol and ethanol oxidation. They concluded that for methanol oxidation, non-alloyed Pt–SnO_x or partially alloyed Pt–Sn catalysts can be used while for ethanol oxidation the usage of fully alloyed Pt_3Sn catalysts is preferred. Also the dehydrogenation reaction of alkanes on Pt clusters showed higher activity with the addition of Sn. The effect of Sn addition on the structural and electronic properties of Pt has been explored by various groups. It has been shown that incorporation of Sn can strongly enhance electro-catalytic activity of Pt [10] and lower the poisoning of the catalyst [11, 13]. Zhou et al. [12]. have found that Sn can enhance ethanol electro-oxidation activity of Pt mostly in the form of Pt_1Sn_1/C, better than Pt_1Ru_1/C and also lengthen the Pt–Pt bonds.

In bulk, platinum tend to alloy with tin to form face-centered-cubic (fcc) phase of Pt_3Sn or hexagonal-closed-packed (hcp) phase of PtSn [19, 20]. Jeyabharathi et al. [21] synthesized carbon-supported Pt–Sn catalyst by simple polyol reduction process. The as-prepared Pt–Sn bimetallic nanoparticles exhibited a single fcc phase of Pt and heat-treatment led to fcc phase of Pt_3Sn and hcp phase of PtSn [19, 21]. Boucher et al. studied the structural and electrochemical properties of Pt–Sn nanoparticle catalysts supported onto carbon with relatively narrow size distribution of 2.4 ± 0.9 nm, while the Pt/Sn ratio was found to be 3:1 at room temperature [22]. With the carbonyl route, they found that the nanoparticles have a certain degree of surface disorder, thus enhancing the electrocatalytic activity for hydrogen adsorption. It was also found that the unique phase of Pt_3Sn alloy can be obtained spontaneously regardless of the amount of tin added [23]. However, Pt–Sn nanoparticles and bulk alloys are known to have segregation of Sn on the surface

and it is important to have Pt rich nanoparticles for good catalytic activity [24, 25]. As we shall show, surface segregation of Sn in nanoparticles of Pt_3Sn leaves patches of Pt atoms exposed to surface and that could lead to higher activity.

Earlier theoretical studies on adsorption or reaction mechanism of Pt–Sn solid surfaces or nanoparticles have been mainly carried out using slab models. For instance, the adsorption of simple alkenes on Pt(111) and surfaces of Pt–Sn alloys [26], hydrogenation of 2-butenyl on Pt(111), and hydrogenation of butadiene on Pt_2Sn/Pt(111) [27] have been studied. Alloying Pt with Sn results in a charge transfer toward Pt and this could further facilitate charge transfer to reactants and their dissociation in a reaction [27].

Despite intensive experimental studies on Pt–Sn nanoclusters [21, 22, 28–34], little is known about the binary Pt–Sn alloy clusters from the theoretical point of view. To date, only the lowest-energy structures and electronic properties of elementary platinum [35–47] and tin clusters [48–55] have been explored using first-principles approaches. To gain insight into Pt–Sn nanoalloys, here we determine the lowest-energy structures of Pt_nSn_n ($n = 1–10$) and $Pt_{3m}Sn_m$ ($m = 1–5$) clusters and discuss the effects of cluster size and composition on the atomic structures and electronic properties. It is found that Pt and Sn atoms tend to mix together, forming nanoscale alloys with bulk-like structural units. In the equilibrium cluster isomers, Pt atoms usually stay inside and form an interior core, while Sn atoms distribute dispersedly on the exterior surface. This may account for the enhanced catalytic behavior of Pt–Sn binary clusters. Due to the limitation of computational resource for an ab initio global search, we focus here on the understanding of the properties of small clusters of Pt_nSn_n ($n = 1–10$) and $Pt_{3m}Sn_m$ ($m = 1–5$) and we believe that some of the conclusions arrived here would be relevant to larger nanoparticles.

Computational Methods

The low-energy isomers of Pt_nSn_n ($n = 1–10$) and $Pt_{3m}Sn_m$ ($m = 1–5$) clusters were globally searched using genetic algorithm (GA) combined with the first principles DMol^3 program. As one of the most widely adopted global optimization algorithms [56], GA and its variations have been intensively used in cluster science. Our group has recently combined GA with DFT calculations and this GA–DFT scheme has been successfully applied to Ga [57], Na [58], Na–Si [59], $(WO_3)_n$ [60], and Au–Ag [61] clusters. Previously, empirical GA search has also been employed to determine the global minimum structures of Pt_n ($n = 15–24$) clusters by Wang and Tian [46].

In the present work, the GA search [62] was started with an initial population with 24 structures, which were randomly generated by choosing a set of initial coordinates for each of them. With 50 % probability, two individuals in the population were chosen as parents to produce a new offspring, (namely "child") via a "cut and spice" mating operation. With another 50 % probability, mutation operation was applied to a randomly selected individual with two types of operations: (1) giving each atom of the cluster a small random displacement with amplitude up to 0.2 Å, and (2) exchanging the atom type within a pair of different atoms (i.e., Pt–Sn pair here). At

each GA iteration, the child cluster was relaxed by DFT optimization. In order to keep the diversity of the populations, the locally stable child was selected to replace one of the individuals if they share the same value of inertia I (the tolerance for the inertia difference is less than 0.04 × atomic number), otherwise the new structure having an inertia different from all the existing isomers, replaced the highest energy isomer by the new one. Here the inertia is defined [59] as $I = \Sigma m_i r_i^2$, where r_i is the distance of the ith atom from the cluster center of mass and m_i is the mass of the ith atom. For each cluster size, we performed more than 1,000 GA iterations to ensure that the global minimum on the potential energy surface is obtained. The specific number of GA iterations generally increases with the cluster size, and relies on the specific chemical composition of the cluster.

DFT calculations were performed using the DMol^3 program with the double numerical basis including d-polarization function (DND) and the Perdew–Wang 91 (PW91) functional within generalized gradient approximation (GGA). The convergence criterion for the self-consistent field calculations was 10^{-6} Ha. Orbital cutoff was chosen as 6.5 Å. All the cluster geometries were fully optimized without any symmetry constraint with the convergence criteria of 0.002 Ha/Å on force and 0.005 Å on displacement. Vibrational analysis on the low-energy isomers of these clusters was carried out to ensure that there are no imaginary frequencies corresponding to the saddle points on the potential energy surface. We have examined possible high-spin states for the low-lying isomers after the structural isomers are determined. All Pt–Sn clusters considered here are non-magnetic.

The above theoretical setting was tested by calculating the dimers of platinum and tin, respectively. In Table 1 we have compared the experimental and theoretical

Table 1 Comparison of the calculated results obtained by using PW91 functional in GGA and DND basis set with the available experimental data for Pt and Sn dimers and solids

	PW91/DND	Experiment
Pt_2 dimer		
E_b (eV/atom)	1.918	1.63
Frequency (cm^{-1})	235.5	215 ± 15 [63]
Bond length (Å)	2.350	2.33 [64]
Electron affinity (eV)	2.122	1.898 ± 0.008 [63]
Pt solid		
a (Å)	3.914	3.9233 [65]
Cohesive energy (eV)	6.160	5.84
Sn_2 dimer		
E_b (eV/atom)	1.269	0.964
Frequency (cm^{-1})	182.1	186 ± 15 [66]
Bond length (Å)	2.820	2.746 [66]
Electron affinity (eV)	1.629	1.962 ± 0.010 [66]
Sn solid		
a (Å)	6.006	5.8316 [65]
b (Å)	3.198	3.1815 [65]
Cohesive energy (eV)	3.077	3.14

results of the binding energy (E_b), vibrational frequency, bond length, and electron affinity. Although E_b is systematically overestimated, the overall agreement between PW91/DND results and experimental data is satisfactory and shows the validity of the present computational method.

For a Pt_xSn_y cluster, we define E_b as:

$$E_b = [(xE_{Pt} + yE_{Sn}) - E_{Pt_xSn_y}]/(x + y), \quad (1)$$

where E_{Pt} (E_{Sn}) is the total energy of a platinum (tin) atom. $E_{Pt_xSn_y}$ is the total energy of the Pt_xSn_y cluster while x and y represent the number of Pt and Sn atoms, respectively. Furthermore, the thermodynamic stability of Pt_nSn_n and $Pt_{3m}Sn_m$ clusters can be characterized by the formation energy (E_{form}), which is defined by:

$$E_{form} = (E_{Pt_nSn_n} - E_{PtSn} \times n)/n, \quad (2)$$

for Pt_nSn_n clusters and

$$E_{form} = (E_{Pt_{3m}Sn_m} - E_{Pt_3Sn} \times m)/m, \quad (3)$$

for $Pt_{3m}Sn_m$ clusters. Here $E_{Pt_nSn_n}$ and $E_{Pt_{3m}Sn_m}$ are the total energies per formula for the Pt_nSn_n and $Pt_{3m}Sn_m$ clusters, E_{PtSn} and E_{Pt_3Sn} are the total energies per formula for the PtSn and Pt_3Sn solids while m and n represent the number of Sn atoms in the two types of clusters, respectively.

To further verify the GA–DFT scheme, we selected Pt_5Sn_5 cluster as a representative to search the ground state structure in an alternative way, i.e., by performing simulated annealing (SA) with first-principles molecular dynamic (FPMD) as implemented in the Vienna Ab initio Simulation Package (VASP) [67] with plane wave basis (200 eV cutoff) and ultrasoft pseudopotentials. The initial cluster structure was generated in a random way and the system was annealed from 2,000 to 300 K stepwise by decreasing the temperature in steps of 100 K. At each temperature, FPMD simulation in the NVT ensemble lasted for 10 ps with a time step of 1 fs. Thus, the total simulation time reaches 180 ps. The final geometry for Pt_5Sn_5 cluster from SA–FPMD search is identical to that from GA–DFT search, assessing the reliability of our global search approach.

Results and Discussion

Low-Energy Structures

The ground state geometries of Pt_nSn_n ($n = 1$–10) and $Pt_{3m}Sn_m$ ($m = 1$–5) clusters are globally searched by GA combined with DFT optimization. The lowest-energy structures and some low-lying isomers are displayed in Figs. 1, 2 and 3 and these are discussed in details below. The coordinates and some properties are given in supporting information.

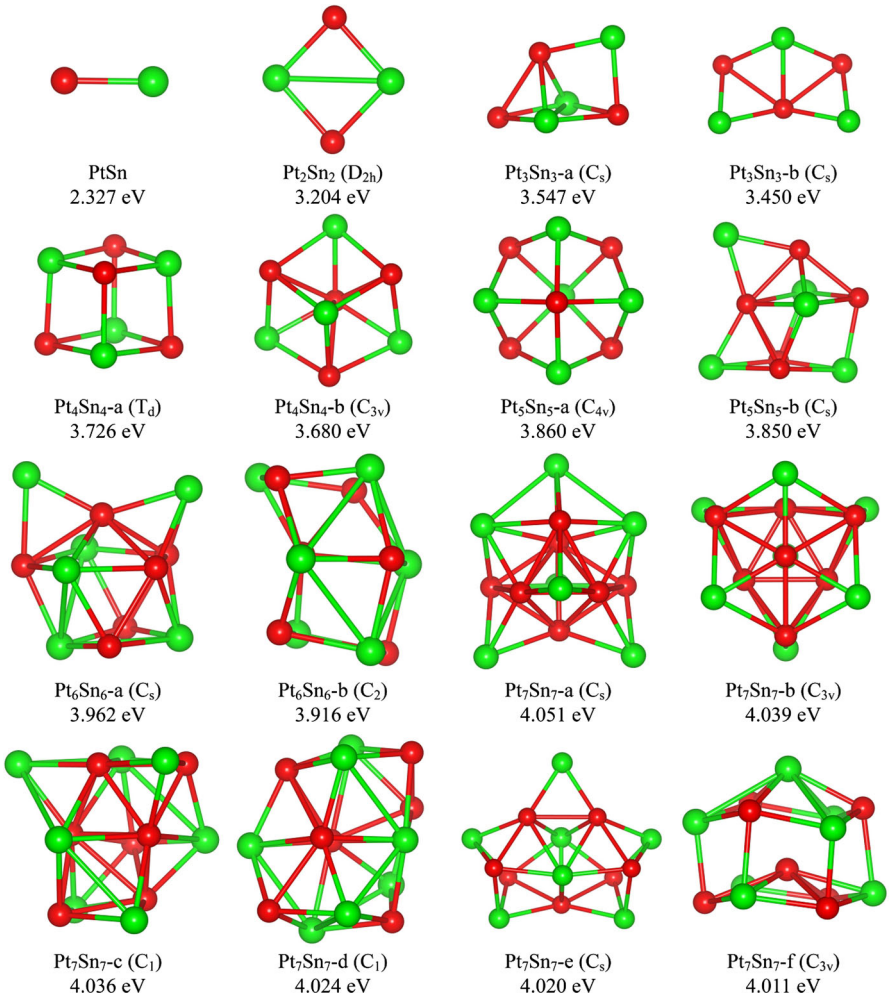

Fig. 1 Low-lying structures of Pt_nSn_n clusters with n = 1–7. The isomers of Pt_nSn_n are listed in the sequence of decreasing binding energy and are marked as *a*, *b*,…. The binding energy per atom (E_b) is given below the name of the cluster and the symmetry is given in the *brackets*. *Red* (*green*) *balls* represent platinum (tin) atoms (Color figure online)

Pt_nSn_n (n = 1–10) Clusters

From our DFT optimization at PW91/DND level, the equilibrium bond length of diatomic PtSn cluster is 2.399 Å, which is slightly longer than the Pt–Pt bond (2.35 Å) and smaller than the Sn–Sn bond (2.82 Å). This can be easily understood because the atomic radius of tin atom is larger (1.58 Å) compared with that of a platinum atom (1.39 Å) [68]. The binding energy of a PtSn dimer is 2.327 eV/atom, which is higher than the values for Pt_2 (1.918 eV/atom) and Sn_2 (1.269 eV/atom). The energy gained by forming a Pt–Sn bond can be evaluated from:

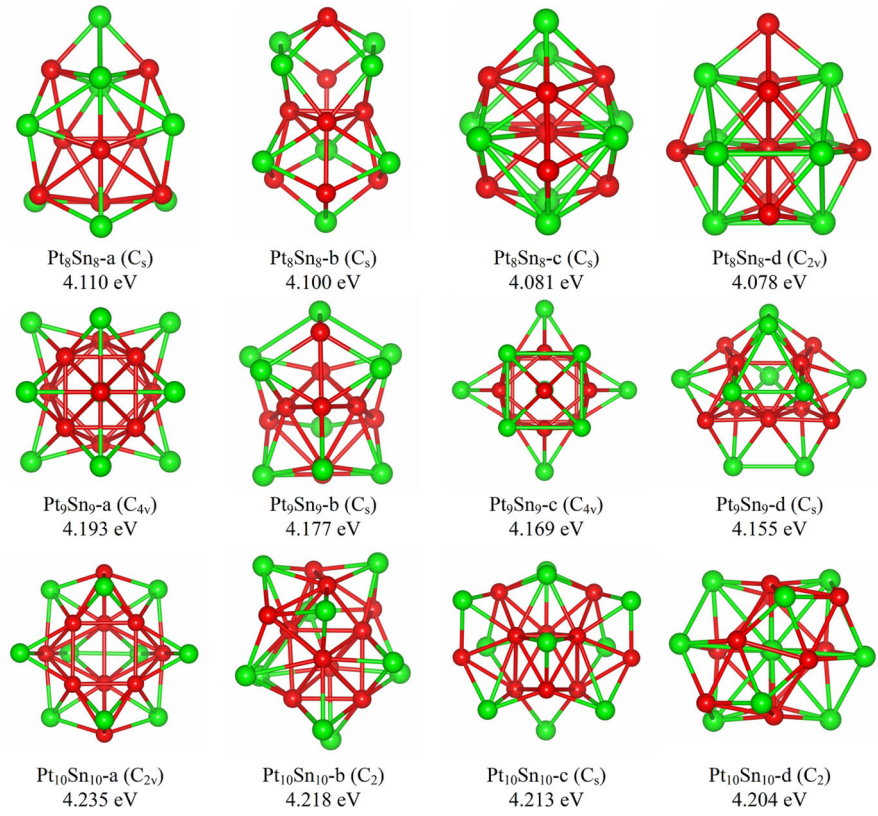

Fig. 2 Low-lying isomers of Pt_nSn_n clusters with n = 8–10. Other details are the same as in Fig. 1 (Color figure online)

$$E_{bond} = 2 \times E_{Pt-Sn} - E_{Sn_2} - E_{Pt_2} = 2 \times 2.327 - 1.269 - 1.918 = 1.467 \text{ eV}. \quad (4)$$

One can clearly see that the formation of Pt–Sn bonds is energetically preferred over the formation of individual Pt–Pt and Sn–Sn bonds, implying that the alloying of Pt and Sn atoms is favorable in binary Pt–Sn clusters, as we will further show in the following discussion.

Figure 1 shows the lowest-energy structures of Pt_nSn_n clusters with n = 1–7, along with some low lying structural isomers. The most stable structure of Pt_2Sn_2 has D_{2h} symmetry, in which the two Pt atoms are connected to two Sn atoms in the middle, forming a rhombus structure with Pt–Sn bond length of 2.574 Å. The distance between the two tin atoms is 3.475 Å. The Sn–Pt–Sn and Pt–Sn–Pt bond angles are 84.903° and 95.097°, respectively.

Starting from Pt_3Sn_3, the Pt–Sn binary clusters prefer to adopt three-dimensional structures. The ground state structures of Pt_3Sn_3 has C_s symmetry, in which two Pt atoms and two Sn atoms form a tetrahedron and a Pt–Sn dimer is capped on a face. In this structure, there is only one Pt–Pt bond of 2.681 Å and a rather long Sn–Sn bond of length 3.398 Å, whereas the average length of the eight Pt–Sn bonds is

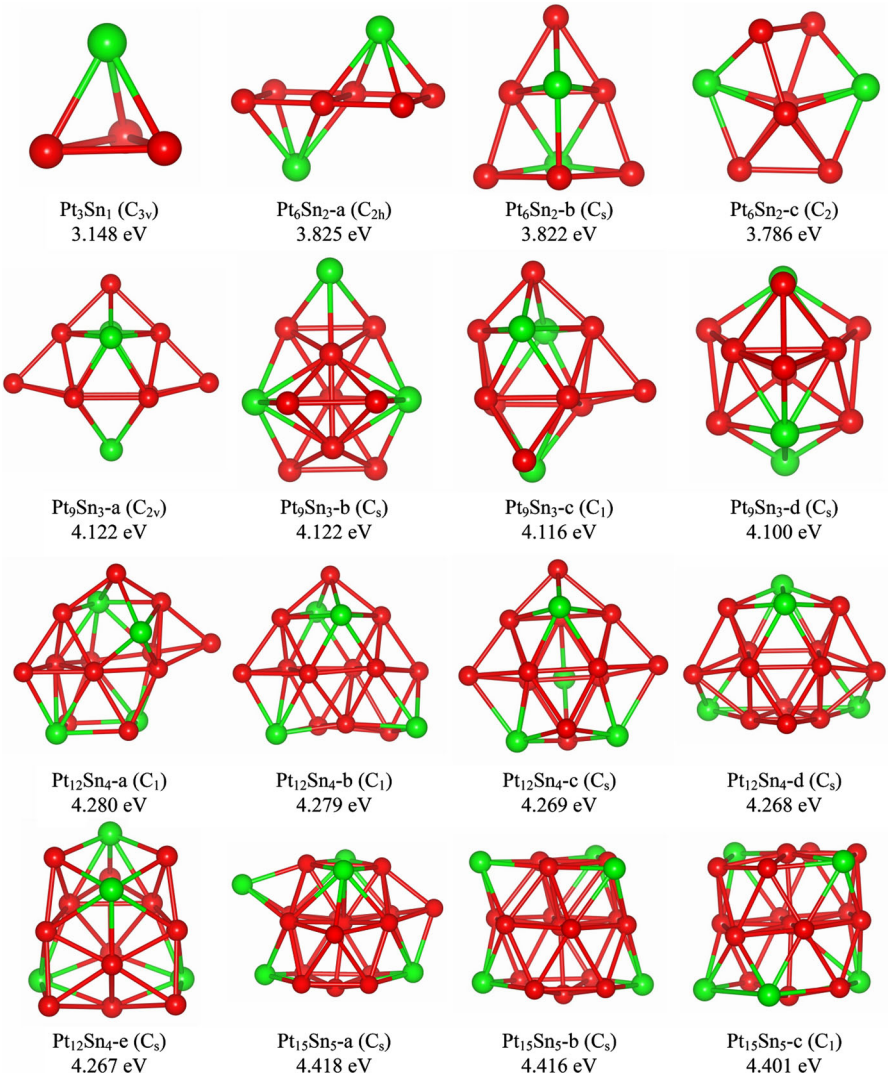

Fig. 3 Low-lying isomers of $Pt_{3m}Sn_m$ clusters with m = 1–5. Other details are the same as in Fig. 1 (Color figure online)

2.662 Å. The latter is shorter than the Pt–Pt bond length and shows the formation of strong Pt–Sn bonds. In addition, we found a metastable C_s isomer (Pt_3Sn_3-b in Fig. 1) that is higher in energy by 0.582 eV. It is made up of two space quadrilaterals and contains two Pt–Pt bonds (length: 2.736 Å) and seven Pt–Sn bonds (average length: 2.615 Å). Note that Pt_3Sn_3-a has ten bonds while Pt_3Sn_3-b has nine bonds. The larger number of Pt–Sn bonds (eight in isomer a compared with seven in isomer b) may account for the higher stability of the former.

The ground state of Pt_4Sn_4 adopts a cube-like motif with T_d symmetry, in which Pt and Sn atoms arrange alternately with identical Pt–Sn bond length of 2.670 Å.

The equilibrium structures slightly deviates from a perfect cube with the Pt–Sn–Pt and Sn–Pt–Sn bond angles of 93.690° and 86.187°, respectively. Note that similar quadrilateral structural units also exist in the bulk phase of PtSn solid [20] with Pt–Sn bond length of 2.732 Å, Pt–Sn–Pt bond angle of 97.395°, and Sn–Pt–Sn bond angle of 82.605°. The metastable Pt_4Sn_4-b isomer shown in Fig. 1 has C_{3v} symmetry and it lies higher on the potential energy surface by 0.368 eV. This structure can be viewed as a flattened cube with the average Pt–Sn bond length of 2.717 Å.

The lowest-energy structure of Pt_5Sn_5 is a hollow cage with C_{4v} symmetry. One Pt atom and one Sn atom are four-coordinated and occupy two ends of the cage, while the remaining four Pt and four Sn atoms are three-coordinated and stay in the waist of the cage. Again, this structure consists of eight quadrilateral structural units with Pt–Sn–Pt bond angle of 95.108° or 96.682°, and Sn–Pt–Sn bond angle of 77.624° or 76.682°. The bond length between the top Pt (Sn) and the waist Sn (Pt) atoms is 2.686 Å (2.683 Å) and the Pt–Sn bond length in the middle part of the cluster is 2.599 Å. From our GA–DFT search, a C_s isomer (Pt_5Sn_5-b in Fig. 1) is found to be close in energy with $\Delta E = 0.1$ eV only. This can be viewed as an eight-atom C_s cage of Pt_5Sn_3 capped with one Sn atom on the face and one Sn atom on the edge.

The lowest-energy structure of Pt_6Sn_6 (C_s symmetry) can be constructed from a ten-atom C_{3v} cage of Pt_6Sn_4 capped with one Sn atom on the face and one Sn atom on the edge, similar to Pt_5Sn_5-b. Platinum atoms form five Pt–Pt bonds with an average bond length of 2.691 Å and there is no Sn–Sn bond. The average bond length of the nineteen Pt–Sn bonds is 2.712 Å which is slightly longer than that of Pt–Pt bond. This is due to the fact that the mean coordination of Sn atoms is higher in this isomer as compared to the smaller size clusters. The metastable Pt_6Sn_6-b isomer with C_2 symmetry ($\Delta E = 0.552$ eV) follows the cube-like motif and can be achieved by fusing two distorted Pt_4Sn_4 cubes via sharing a Pt_2Sn_2 quadrilateral.

Six isomers of Pt_7Sn_7 cluster are presented in Fig. 1. The most stable one, i.e., Pt_7Sn_7-a can be seen to have an open core–shell structure. Seven Pt atoms form a tricapped tetrahedron with C_{3v} symmetry as the core, whereas three Sn atoms are capped on the Pt triangular faces and the remaining four Sn atoms are capped on the spatial quadrilateral of four Pt atoms in such a way that the seven Sn atoms are separated with the minimum Sn–Sn distance of 3.256 Å. Pt_7Sn_7-b also has the same C_{3v} core of Pt atoms with seven Sn atoms dispersedly capped on the spatial quadrilaterals of Pt_7 core in such a way that the entire cluster retains C_{3v} symmetry. Pt_7Sn_7-c has a three-layered structure with four, five, and five atoms on each layer. Pt_7Sn_7-d isomer can be regarded as two fused cages (Pt_5Sn_3 and Pt_4Sn_5) via sharing a Pt_2Sn triangular face. Pt_7Sn_7-e has a basket-like structure with C_s symmetry, in which two identical eight-atom cages of Pt_4Sn_4 with D_{2d} symmetry are fused together via sharing a $PtSn_2$ triangle and adding a Sn atom on the top. Pt_7Sn_7-f structure also has high symmetry (C_{3v}) and can be viewed as a sphere-like cage with alternate arrangement of Pt and Sn atoms except that one Pt atom sinks into the cage interior.

The ground state structure of Pt_8Sn_8 with C_s symmetry is obtained by capping three Sn atoms on a core structure formed by welding a bicapped pentagonal bipyramid of Pt_6Sn_3 and a spatial quadrilateral of Pt_2Sn_2. The Pt_8Sn_8-b structure consists of two cages sharing a Pt_3 triangle, i.e., a capped square anti-prism of

Pt_5Sn_4 and a ten-atom polyhedron of Pt_6Sn_4. In the Pt_8Sn_8-d structure with C_{2v} symmetry, six Pt and eight Sn atoms constitute a symmetric D_{4h} hollow cage (with twelve spatial quadrilaterals of Pt_2Sn_2), whereas one Pt atom sits in the cage center and the last Pt atom is capped on the surface. Similarly, the Pt_8Sn_8-c structure is based on a fourteen-atom irregular cage of Pt_7Sn_7 with one interior Pt atom inside the cage and one Sn atom capped outside.

The ground state structure of Pt_9Sn_9 has a high symmetry of C_{4v}. It can be regarded as a bicapped square antiprism formed by nine platinum atoms and one tin atom, with eight additional Sn atoms capped on each of the triangular facets of Pt core. Similarly, the Pt_9Sn_9-c isomer also with C_{4v} symmetry is constituted by two fused square anti-prisms (one Pt_8 and one Pt_4Sn_4 via sharing a Pt_4 square) capped with one top Pt atom, one bottom Sn atom, and four Sn atoms on the waist of the lower anti-prism. In the Pt_9Sn_9-b structure, eight Pt atoms constitute a core of bicapped trigonal prism, with one Pt and nine Sn atoms dispersedly distributed around the Pt_8 core, forming a rather open structure. The Pt_9Sn_9-d isomer is a three-layered structure (C_s symmetry). The top layer contains two Pt and two Sn atoms, forming a rhombus; the middle layer is a Pt_4 square edge capped with three Sn atoms; the bottom layer consists of three Pt and four Sn atoms and can be viewed as a buckled Pt-centered hexagon.

$Pt_{10}Sn_{10}$-a can be viewed as a core–shell structure with C_{2v} symmetry, in which ten Pt atoms constitute a tetracapped trigonal prism as the core and ten Sn atoms distribute separately as the outer shell. $Pt_{10}Sn_{10}$-b can also be regarded as a core–shell structure, where the Pt_{10} core is an octahedron with the addition of four Pt atoms. The geometry of $Pt_{10}Sn_{10}$-c is formed by a flat core of $Pt_{10}Sn_3$ with two layers of atoms capped with three Sn atoms on one side and four Sn atoms on the other side. $Pt_{10}Sn_{10}$-d is a stuffed cage with one Sn atom inside and the outer irregular cage is mainly composed of Pt_2Sn_2 rhombuses as basic structural units.

To briefly summarize the structural trend, we find three dimensional (3D) cluster structures that emerge when the number of atoms exceeds four. Pt_2Sn_2 quadrilaterals as basic structural units of PtSn solid are seen in many cluster isomers. Pt and Sn atoms prefer to mix with each other. However, due to the larger size of tin atoms, they tend to segregate and are usually located on the exterior of the cluster and are well separated, while platinum atoms tend to form interior core with Pt–Pt bonds. This is also expected because the cohesive energy of bulk Pt (5.852 eV/atom) is much larger (nearly 1.6×) than the value for bulk Sn (3.12 eV/atom). In clusters E_b increases with size and approaches the value for bulk. Accordingly with increasing size of PtSn clusters, E_b could be higher if more Pt atoms interact together in the core region. Also according to simple theories of surface segregation in alloys the element with lower surface energy (larger atomic size) tends to segregate at the surface in order to minimize the surface free energy. This segregation is less in ordering systems such as in Pt–Sn because segregation of Sn atoms on the surface also has the tendency to pull Pt atoms along with it. Hence, in nanoscale binary PtSn catalysts, Sn can protect Pt sites from being poisoned. Also we can say that Sn blocks some Pt sites such that in general the low lying atomic structures of PtSn clusters have predominantly single or pairs of Pt atoms exposed on the surface. This can enhance those reactions that can take place on a single or pair of Pt atoms,

thereby increasing the reactivity and selectivity. Furthermore, in larger Pt–Sn clusters segregation of Sn may make the catalyst inactive by blocking most of the (active) Pt sites. Therefore for high reactivity control of both the size and composition of the catalyst is important.

$Pt_{3m}Sn_m$ (m = 1–5) Clusters

The structures of $Pt_{3m}Sn_m$ (m = 1–5) clusters are given in Fig. 3. The ground state structure of Pt_3Sn is a typical trigonal pyramid (C_{3v}) with Sn atom capping a Pt_3 triangle, Pt–Sn and Pt–Pt bond lengths being 2.661 Å and 2.556 Å, respectively. The lowest-energy structure of Pt_6Sn_2 (Pt_6Sn_2-a in Fig. 3) with C_{2h} symmetry is obtained by joining two square pyramids (Sn atom on top and four Pt atoms on the basal plane) in opposite directions via sharing one Pt–Pt bond. The Pt_6Sn_2-b isomer with C_s symmetry, lying only 0.024 eV higher than the most stable one, can be regarded as a tricapped trigonal bipyramid in which the two Sn atoms sit on the two vertices of the trigonal bipyramid. Two Pt–Pt bonds in the triangular base are broken (elongated). This structure can also be regarded as capping of a triangular isomer of Pt_6 (the central triangle) on both the faces by Sn atoms. Note that a planar triangular isomer of Pt_6 has the lowest energy and the isomer with two fused squares is a low lying isomer. Pt_6Sn_2-c structure (C_2 symmetry) is a capped pentagonal bipyramid with one broken Pt–Sn side and one capped Pt atom, where the two Sn atoms are located in the pentagonal rim. Note that in all these cases the Sn atoms tend to be far from each other. This means that Pt sites remain available for reaction.

The lowest-energy structure for Pt_9Sn_3 has C_{2v} symmetry and can be constructed by symmetrically face-capping two Pt atoms on the waist of a bicapped square anti-prism. The Pt_9Sn_3-c isomer can be also obtained by face-capping the same bicapped square anti-prism with two Pt atoms but in a different manner (one Pt on the waist and one Pt on the bottom). The structure of the isoenergetic Pt_9Sn_3-b isomer ($\Delta E = 0.01$ eV) is formed by an eleven-atom D_{3h} cage with a Sn atom capping on a platinum triangular face of the cage. Similarly, the Pt_9Sn_3-d isomer can be constructed by capping a Sn atom on an eleven-atom C_s cage consisting of nine Pt atoms and two Sn atoms.

In the case of $Pt_{12}Sn_4$ binary cluster, the most stable structure is rather complicated and can be described as an anomalous hollow cage on which the four Sn atoms are well separated by Pt atoms. A characteristic of the structure in this size range is the formation of face (s) with a centered hexagon (with or without capping) as one finds in the Frank–Kaspar polyhedral structures. There are distortions due to large size mismatch between Pt and Sn atoms. Similar hollow cage with C_s symmetry and dispersed Sn distribution is found as the $Pt_{12}Sn_4$-e isomer, whereas a fourteen-atom flat cage capped with one Pt and one Sn atoms on the top and bottom is obtained as the $Pt_{12}Sn_4$-d isomer. The $Pt_{12}Sn_4$-b structure can be obtained from a capped square antiprism by adding a five-atom layer on the bottom and then capping two Pt atoms on the waist. $Pt_{12}Sn_4$-c is a four-layered structure with C_s symmetry, with one Pt atom, three Pt atoms and one Sn atom, six Pt atoms and one Sn atom, and two Pt atoms and two Sn atoms, on successive layer.

$Pt_{15}Sn_5$-a is a core–shell structure, which consists of a spherical eighteen-atom cage (fourteen Pt atoms and four Sn atoms), one Pt atom stuffed inside the cage and

one Sn atom capped on a triangle facet of Pt atoms. In this structure there is Pt centered hexagon with four Pt atoms and two Sn atoms. This is capped by another Pt centered hexagon of Pt in an anti-prism structure. The remaining six atoms (three Pt and three Sn) are distributed in such a way that a Pt_2Sn_2 quadlateral caps the Pt_7 centered hexagon. Finally one Pt and one Sn atoms cap this whole unit in opposite directions. Both $Pt_{15}Sn_5$-b and $Pt_{15}Sn_5$-c isomers have three-layered structures and have similarity with $Pt_{15}Sn_5$-a isomer. The difference is in the way the remaining six atoms are distributed, the two centered hexagons being the same. In isomer $Pt_{15}Sn_5$-b, three Sn atoms cap a Pt_3 triangle to form a triangular structure that caps the Pt_7 centered hexagon. Thus within each layer, Sn atoms are separated by Pt atoms. Note that there is resemblance with the structural motif of Pt_3Sn bulk solid. The $Pt_{15}Sn_5$-b is less stable than $Pt_{15}Sn_5$-a by only 0.04 eV and $Pt_{15}Sn_5$-a can also be viewed as a three-layered structure with a capped atom and some distortion. Hence, the bulk-like structure already emerges at the size of $Pt_{15}Sn_5$.

Similar to the cases of Pt_nSn_n clusters, the Pt and Sn atoms prefer to mix together in $Pt_{3m}Sn_m$ ($m = 1$–5) clusters also. With more number of Pt atoms, the Sn atoms are well separated without forming any Sn–Sn bond. The tendency to form Pt triangular faces is easily seen and this would accelerate reactions in which interaction with up to three Pt atoms is required. As the cluster grows larger, there is a clear tendency of layered structures consisting of Pt–Sn alternative triangular lattices, which resemble the Pt_3Sn solid.

Bond Length and Bond Strength

Figure 4 presents the average Pt–Sn and Pt–Pt bond lengths for the lowest energy isomers of Pt_nSn_n ($n = 1$–10) and $Pt_{3m}Sn_m$ ($m = 1$–5) clusters. Generally, both Pt–Sn and Pt–Pt bond lengths increase with the increasing number of atoms for both the types of binary clusters as the coordination number also increases. However, for the Pt_nSn_n clusters, the rising trend of Pt–Sn bond length is much more pronounced than that of the Pt–Pt one. When the total number of atoms reaches 12 (i.e., $n \geq 6$), the average bond lengths of Pt–Sn and Pt–Pt approximately approach their bulk values in the case of PtSn alloy. The variation in bond lengths is in accordance with the analysis of Mayer bond order (MBO) [69], i.e., a shorter bond corresponds to a higher bond order. For example, the average MBO of Pt–Sn bonds in the Pt_2Sn_2 cluster is 1.203, and it reduces to 0.876 for Pt_3Sn_3, 0.832 for Pt_4Sn_4, 0.658 for Pt_6Sn_6, and 0.534 for $Pt_{10}Sn_{10}$. Meanwhile, the MBO values of Pt–Pt bonds are 0.719 for Pt_3Sn_3, 0.471 for Pt_6Sn_6, and 0.355 for $Pt_{10}Sn_{10}$. For a given Pt_nSn_n cluster, the MBO parameter for Pt–Sn bonds is larger than that of Pt–Pt bonds by about 0.2, suggesting stronger Pt–Sn bonds compared with Pt–Pt ones.

In the case of the $Pt_{3m}Sn_m$ clusters, the Pt–Sn and Pt–Pt bond lengths increase slowly with little oscillation as the cluster size increases. However, even for the largest cluster ($Pt_{15}Sn_5$) we explored, they are still significantly smaller than the bulk values by 0.08 Å for Pt–Sn bond and 0.2 Å for Pt–Pt. For the same total number of atoms, the Pt–Sn bonds in $Pt_{3m}Sn_m$ clusters are generally longer than those in Pt_nSn_n clusters, and the corresponding MBO are smaller. For instance, the Pt–Sn MBO parameters are 0.819 for Pt_3Sn_1, 0.586 for Pt_6Sn_2, 0.514 for Pt_9Sn_3, 0.525 for $Pt_{15}Sn_5$. On the contrary,

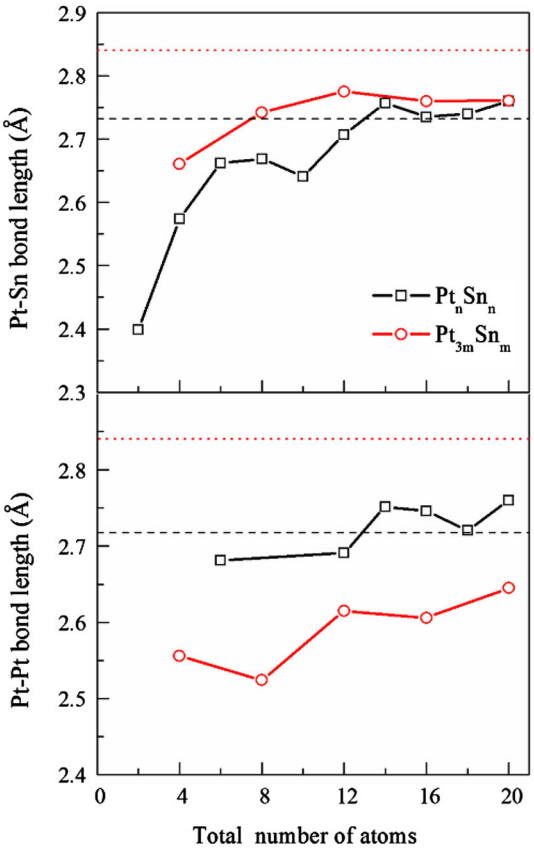

Fig. 4 Average Pt–Sn and Pt–Pt bond lengths for the lowest-energy isomers of Pt_nSn_n (n = 1–10) and $Pt_{3m}Sn_m$ (m = 1–5) clusters as a function of the total number of atoms. The *black dashed* and *red dot lines* show the bond lengths in bulk PtSn and Pt_3Sn, respectively (Color figure online)

the lengths of Pt–Pt bonds in $Pt_{3m}Sn_m$ clusters are generally shorter than those in Pt_nSn_n clusters and the MBO values for Pt–Pt bonds are larger (0.852 for Pt_3Sn_1, 0.65 for Pt_9Sn_3, 0.539 for $Pt_{15}Sn_5$). For a given $Pt_{3m}Sn_m$ cluster, the bond strengths of Pt–Sn and Pt–Pt bonds as characterized by the MBO are comparable. As a consequence, Pt and Sn atoms are able to form close-packed structures composed of triangular layers. Note that in bulk Pt_3Sn solid, the Pt–Pt and Pt–Sn distances are identical with Pt and Sn atoms situated on a fcc lattice alternately.

Relative Stability and Electronic Properties

The formation energy and E_b of Pt_nSn_n (n = 1–10) and $Pt_{3m}Sn_m$ (n = 1–5) clusters are plotted as a function of the total number of atoms in Fig. 5. It can be seen that the bigger the cluster size is, the more stable it is, as evidenced by the lower formation energy and higher E_b with the growing cluster size. Moreover, the rising trend of E_b becomes slower as the number of atoms exceeds ten. According to the computed formation energies, a Pt_nSn_n cluster is energetically more favorable than a $Pt_{3m}Sn_m$ cluster with the same total number of atoms.

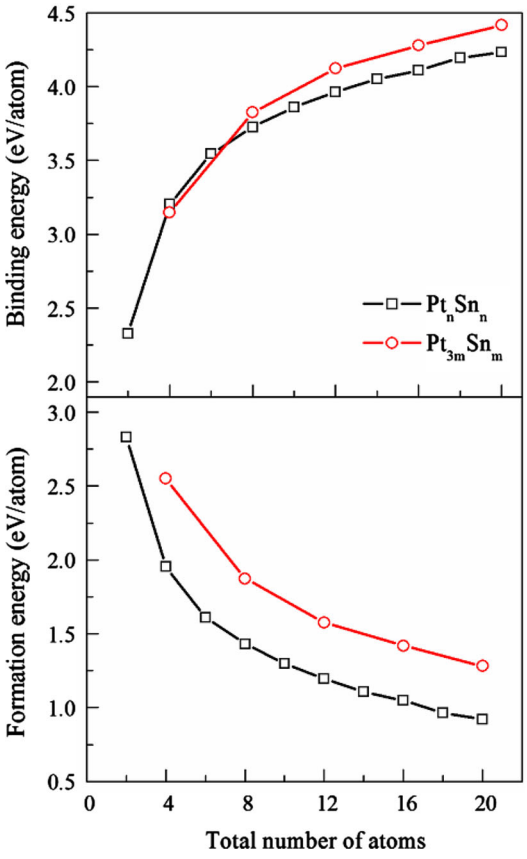

Fig. 5 The binding energy (*upper*) and the formation energy (*lower*) of Pt_nSn_n (n = 1–10) and $Pt_{3m}Sn_m$ (m = 1–5) clusters versus the total number of atoms in a cluster. The *black line* with *squares* represents Pt_nSn_n while *the red line* with *circles* stands for $Pt_{3m}Sn_m$ clusters (Color figure online)

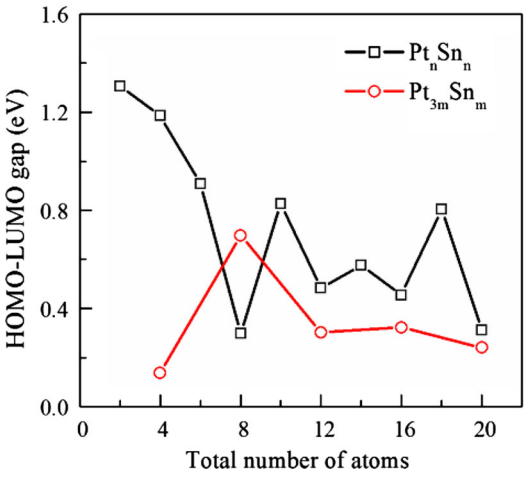

Fig. 6 HOMO–LUMO gap as a function of the total number of atoms in Pt_nSn_n (n = 1–10) clusters and $Pt_{3m}Sn_m$ (m = 1–5) clusters. The *black line* with *squares* represents Pt_nSn_n while the *red line* with *circles* stands for $Pt_{3m}S_m$ (Color figure online)

The electronic properties of the binary Pt_nSn_n and $Pt_{3m}Sn_m$ clusters are discussed in terms of the highest occupied molecular orbital–lowest unoccupied molecular orbital (HOMO–LUMO) gaps, density of states (DOS), Mülliken charge, and molecular orbitals. From the curve of the HOMO–LUMO gap (Fig. 6), one can see distinct even–odd oscillation for Pt_nSn_n clusters with $n \geq 3$. Moreover, Pt_2Sn_2 and Pt_4Sn_4 clusters possess relatively large energy gaps of more than 1 eV. The HOMO–LUMO gaps for Pt_nSn_n clusters are usually larger than the values for $Pt_{3m}Sn_m$ clusters. This is due to larger number of Pt atoms and therefore more electronic states in $Pt_{3m}Sn_m$ clusters compared with Pt_nSn_n clusters with the same number of atoms. As we shall show, some of the *d* states remain unoccupied particularly for $Pt_{3m}Sn_m$ clusters. For clusters with up to twenty atoms, the HOMO–LUMO gaps for both $Pt_{10}Sn_{10}$ and $Pt_{15}Sn_5$ clusters become small, i.e., about 0.2–0.3 eV, approaching the

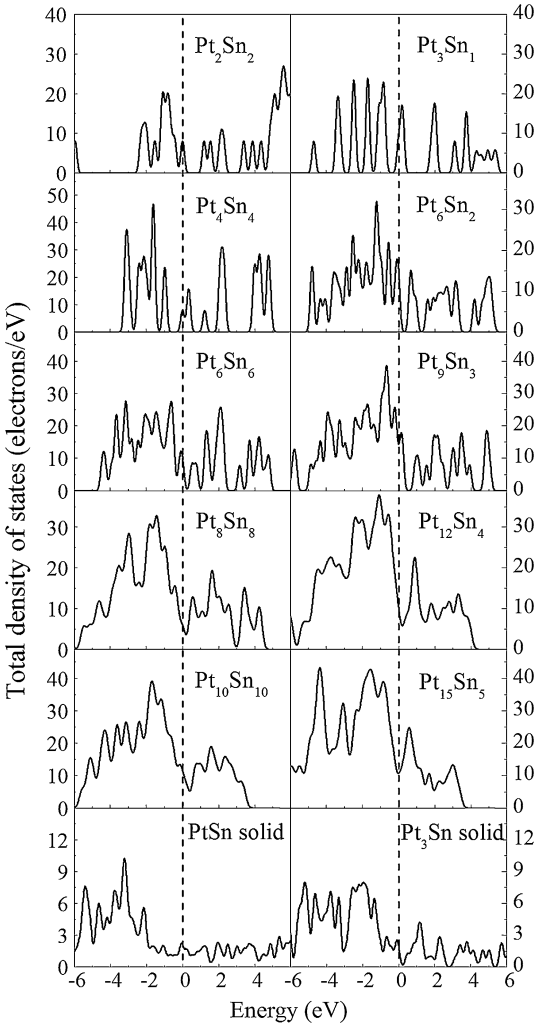

Fig. 7 The density of states for selected Pt_nSn_n (n = 1–10) clusters and $Pt_{3m}Sn_m$ (m = 1–5) clusters. For comparison, the total number of atoms in the two types of clusters is taken to be the same for different m. The HOMO (Fermi energy for bulk) is marked with *dashed line*

bulk limit of zero gap for metallic PtSn and Pt_3Sn alloys. These values should, however, be considered as underestimation due to the use of GGA.

The total DOS of Pt_nSn_n (n = 1–10) and $Pt_{3m}Sn_m$ (m = 1–5) clusters for selected sizes such that the total number of atoms is the same in the two types of clusters, are presented in Fig. 7, and these are compared with those of the bulk PtSn and Pt_3Sn solids. One can see that the small clusters such as Pt_2Sn_2, Pt_3Sn_1, and Pt_4Sn_4 exhibit molecular-like discrete electronic states. As the cluster size grows (with more than 12 atoms), the discrete states become densely distributed and the features of the DOS start resembling those for the bulk. Starting from Pt_8Sn_8 and $Pt_{12}Sn_4$, the main peaks in the total DOS shift towards higher binding energy with increasing size, and gradually approach the bulk behavior. However, there are noticeable differences in the vicinity of the HOMO and this is likely to have important effect on the reactivity of the clusters.

The detailed hybridization between Pt and Sn atoms can be analyzed from the partial DOS shown in Fig. 8 for Pt_4Sn_4 and Pt_6Sn_2 as representatives. Obviously, the total DOS in the vicinity of the HOMO has the main contribution from the *d* states

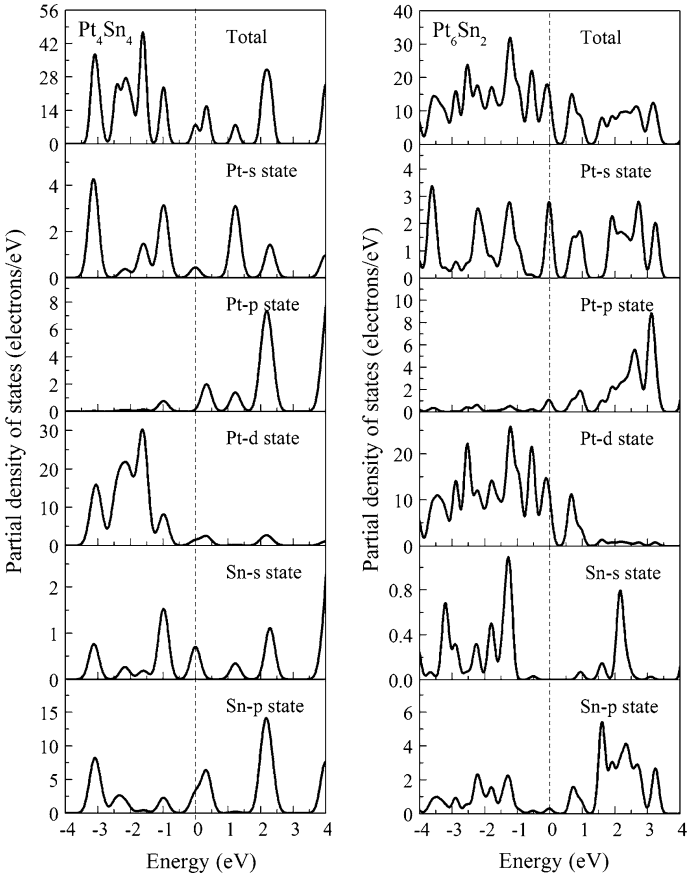

Fig. 8 Partial densities of states for Pt_4Sn_4 and Pt_6Sn_2 clusters

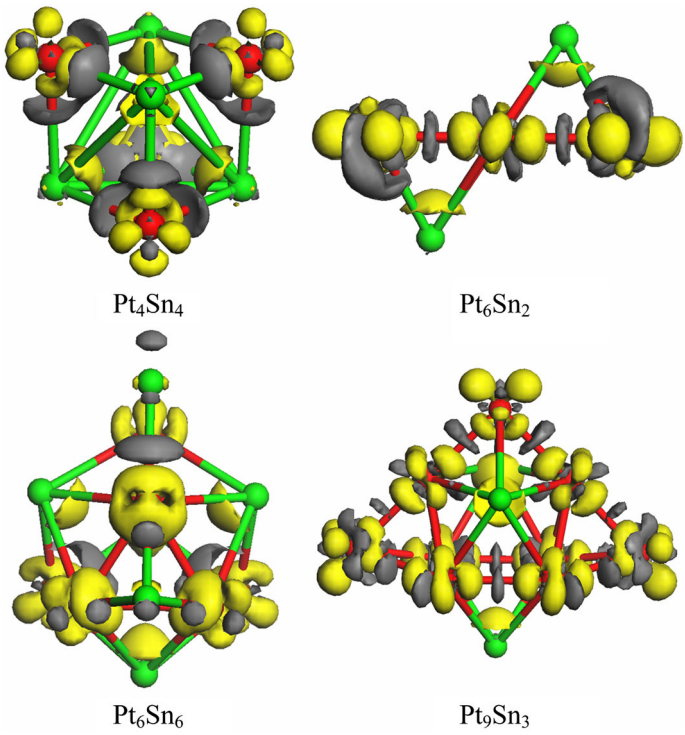

Fig. 9 Charge density differences for Pt_4Sn_4, Pt_6Sn_2, Pt_6Sn_6 and Pt_9Sn_3 clusters. The *gray areas* correspond to electron deficiency, while the *yellow ones* mean electron accumulation (Color figure online)

of Pt atoms and *p* states of Sn atoms. For the occupied bonding states, there is clear correspondence between the Pt-*d* states and Sn-*p* states, suggesting strong *p*–*d* hybridization. However, for the unoccupied anti-bonding states, we observe some hybridization between the Pt-*p* orbitals and Sn-*p* orbitals. The finding of *p*–*d* interaction is supported by the strong Pt–Sn bond energy and larger Mayer bond order mentioned above. Mülliken charge analysis further demonstrates that each Sn atom donates about 0.4–0.5 (0.45–0.7) electrons to Pt atoms in the Pt_nSn_n ($Pt_{3m}Sn_m$) clusters. This is also a reason why Sn atoms tend to be well separated. Further analysis of charge density differences of selected Pt–Sn clusters (Fig. 9) demonstrates that the electron-deficiency area is located on the Pt–Sn bonds, while there is some electron accumulation around the Pt atoms. This can be easily explained by the electronegativities of these two elements (2.28 for Pt and 1.96 for Sn, according to Pauling). Previous first-principles calculations also revealed that alloying Pt with Sn results in a small charge transfer from Sn to Pt [27].

Figure 10 gives the representative frontier orbitals (HOMO−1, HOMO, LUMO, and LUMO+1) for four selected clusters, i.e., Pt_4Sn_4, Pt_6Sn_2, Pt_6Sn_6, and Pt_9Sn_3. Clearly, all these orbitals are rather delocalized and their spatial shapes show typical *d* characteristics. Also note that the frontier orbitals are mainly located on the Pt atoms rather than on the Sn atoms. This can be related to the partial DOS in Fig. 8 (in which the electronic states near the HOMO level mainly originate from the

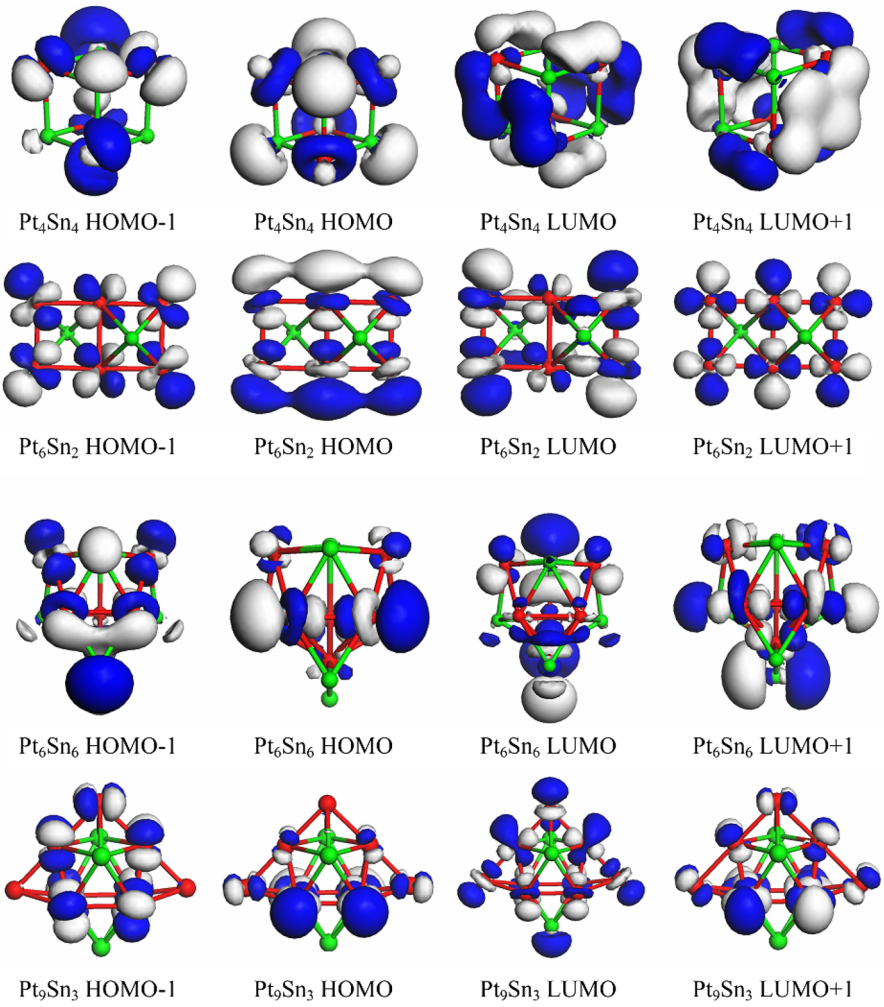

Fig. 10 Isosurfaces for HOMO−1, HOMO, LUMO, and LUMO+1 of Pt_4Sn_4, Pt_6Sn_2, Pt_6Sn_6, and Pt_9Sn_3 clusters. *Green (red) balls* represent tin (platinum) atoms. The *blue and white isosurfaces* denote the wave function phases (Color figure online)

d states of Pt atoms). The results of Mülliken charge analysis show that Sn atoms donate electrons to Pt atoms. Therefore, in the binary Pt–Sn nanocatalysts, the Pt atoms with enriched electrons would serve as active site, whereas the role of Sn atoms is to separate and protect the Pt atoms.

Conclusions

To summarize, we have carried out unbiased global search of the Pt_nSn_n (n = 1–10) and $Pt_{3m}Sn_m$ (m = 1–5) clusters using DFT calculations combined with genetic

algorithm to investigate their low-lying atomic structures and electronic properties. Due to strong *p–d* hybridization, Pt and Sn atoms form strong Pt–Sn bonds in the binary clusters and tend to mix well. For Pt_nSn_n clusters, Pt atoms usually stay inside the cluster interior while Sn atoms prefer to distribute on the exterior sites. In the case of $Pt_{3m}Sn_m$, we observed bulk-like layered structures with alternate Pt/Sn distribution on a triangular lattice. Analysis of the bond length and Mayer bond order show that the Pt–Sn bonds are stronger than Pt–Pt ones in the Pt_nSn_n clusters and the bond strength decreases with increasing cluster size. However, in the $Pt_{3m}Sn_m$ clusters, the strength of Pt–Pt and Pt–Sn bonds are comparable and less sensitive to the cluster size. The electronic states near the HOMO have the main contribution from the *d* states of Pt atoms and *p* states of Sn atoms, while the HOMO and LUMO are delocalized and show *d* characteristics. In the Pt–Sn binary clusters, Pt atoms as active sites are separated and have different distributions in Pt_nSn_n and $Pt_{3m}Sn_m$ clusters. Pt_nSn_n clusters tend to get coated by the Sn atoms often leaving single or pairs of Pt atoms for reaction. On the other hand in $Pt_{3m}Sn_m$ clusters more Pt atoms are available for reaction such as triangular faces. In general Pt atoms accept extra electrons from Sn atoms. This charge transfer is smaller in the case of $Pt_{3m}Sn_m$ clusters. Both the effects namely charge transfer and isolated Pt sites seem to act beneficially for improving the catalytic activity of Pt–Sn catalysts. Our results are likely to be relevant to clusters of other ordering alloys in which the cohesive energy of one component is significantly higher than the value for the other.

Supporting Information

The formation energy, gaps, Mülliken charge on Pt and Sn atoms, bond lengths as well as the number of Pt–Pt, Pt–Sn, and Sn–Sn bonds for Pt_nSn_n ($n = 1–10$) and $Pt_{3m}Sn_m$ ($m = 1–5$) clusters. For the latter there are no Sn–Sn bonds. Cartesian coordinates of all the clusters are listed in Table S3. This material is available free of charge via the Internet at http://pubs.acs.org.

Acknowledgments This work was supported by the National Natural Science Foundation of China (No. 11134005, 11304030), the Fundamental Research Funds for the Central Universities of China (No. DUT14LK19).

References

1. D. Sanfilippo (2000). *CATTECH* **4**, 56.
2. N. Alonso-Vante (2010). *Chemphyschem* **11**, 2732.
3. U. A. Paulus, A. Wokaun, G. G. Scherer, T. J. Schmidt, V. Stamenkovic, V. Radmilovic, N. M. Markovic, and P. N. Ross (2002). *J. Phys. Chem. B* **106**, 4181.
4. L. Dubau, J. Durst, F. Maillard, L. Guétaz, M. Chatenet, J. André, and E. Rossinot (2011). *Electrochim. Acta* **56**, 10658.
5. S. R. Calvo and P. B. Balbuena (2007). *Surf. Sci.* **601**, 165.
6. H. W. Lei, S. Suh, B. Gurau, B. Workie, R. X. Liu, and E. S. Smotkin (2002). *Electrochim. Acta* **47**, 2913.

7. L. Dubau, F. Hahn, C. Coutanceau, J. M. Léger, and C. Lamy (2003). *J. Electroanal. Chem.* **554–555**, 407.
8. H. Wang, Z. Jusys, and R. J. Behm (2006). *J. Appl. Electrochem.* **36**, 1187.
9. M. S. Löffler, H. Natter, R. Hempelmann, and K. Wippermann (2003). *Electrochim. Acta* **48**, 3047.
10. Y. Wang, S. Song, G. Andreadis, H. Liu, and P. Tsiakaras (2011). *J. Power Sources* **196**, 4980.
11. W. Qi, G. Q. Sun, L. H. Jiang, M. Y. Zhu, G. X. Wang, X. Qin, S. G. Sun, Q. S. Chen, Y. X. Jiang, and S. P. Chen (2008). *Spectrosc. Spectr. Anal.* **28**, 47.
12. W. J. Zhou, W. Z. Li, S. Q. Song, Z. H. Zhou, L. H. Jiang, G. Q. Sun, Q. Xin, K. Poulianitis, S. Kontou, and P. Tsiakaras (2004). *J. Power Sources* **131**, 217.
13. C. Lamy, S. Rousseau, E. M. Belgsir, C. Coutanceau, and J. M. Léger (2004). *Electrochim. Acta* **49**, 3901.
14. F. Colmati, E. Antolini, and E. Gonzalez (2008). *J. Solid State Electrochem.* **12**, 591.
15. E. Antolini and E. R. Gonzalez (2011). *Catal. Today* **160**, 28.
16. G. Meitzner, G. H. Via, F. W. Lytle, S. C. Fung, and J. H. Sinfelt (1988). *J. Phys. Chem.* **92**, 2925.
17. D. H. Lim, D. H. Choi, W. D. Lee, and H. I. Lee (2009). *Appl. Catal. B* **89**, 484.
18. D. Rodríguez, J. Sanchez, and G. Arteaga (2005). *J. Mol. Catal. A* **228**, 309.
19. Z. Paál, A. Wootsch, D. Teschner, K. Lázár, I. E. Sajó, N. Győrffy, G. Weinberg, A. Knop-Gericke, and R. Schlögl (2011). *Appl. Catal. A* **391**, 377.
20. P. Villars *Pearson's Handbook of Crystallographic Data for Intermetallic Phases*, vol. 1 (American Society for Metals, Metals Park, 1986).
21. C. Jeyabharathi, P. Venkateshkumar, J. Mathiyarasu, and K. L. N. Phani (2008). *Electrochim. Acta* **54**, 448.
22. A. C. Boucher, N. Alonso-Vante, F. Dassenoy, and W. Vogel (2003). *Langmuir* **19**, 10885.
23. M. Boualleg, D. Baudouin, J.-M. Basset, F. Bayard, J.-P. Candy, J.-C. Jumas, L. Veyre, and C. Thieuleux (2010). *Chem. Commun.* **46**, 4722.
24. V. Kumar (1981). *Phys. Rev. B* **23**, 3756.
25. V. Kumar and K. H. Bennemann (1984). *Phys. Rev. Lett.* **53**, 278.
26. C. Becker, J. Haubrich, K. Wandelt, F. Delbecq, D. Loffreda, and P. Sautet (2008). *J. Phys. Chem. C* **112**, 14693.
27. F. Delbecq, D. Loffreda, and P. Sautet (2009). *J. Phys. Chem. Lett.* **1**, 323.
28. P. Bommersbach, M. Chaker, M. Mohamedi, and D. Guay (2008). *J. Phys. Chem. C* **112**, 14672.
29. K. A. Grant, K. M. Keryou, and P. A. Sermon (2008). *Faraday Discuss.* **138**, 257.
30. M. Arenz, V. Stamenkovic, B. B. Blizanac, K. J. Mayrhofer, N. M. Markovic, and P. N. Ross (2005). *J. Catal.* **232**, 402.
31. Z. R. Ismagilov, E. V. Matus, A. M. Yakutova, L. N. Protasova, I. Z. Ismagilov, M. A. Kerzhentsev, E. V. Rebrov, and J. C. Schouten (2009). *Catal. Today* **147**, (Supplement), S81.
32. A. Borgna, S. M. Stagg, and D. E. Resasco (1998). *J. Phys. Chem. B* **102**, 5077.
33. H. Bönnemann, P. Britz, and W. Vogel (1998). *Langmuir* **14**, 6654.
34. Y. Yao, Q. Fu, Z. Zhang, H. Zhang, T. Ma, D. Tan, and X. Bao (2008). *Appl. Surf. Sci.* **254**, 3808.
35. L. L. Wang and D. D. Johnson (2007). *Phys. Rev. B* **75**, 235405.
36. D. Majumdar, D. Dai, and K. Balasubramanian (2000). *J. Chem. Phys.* **113**, 7919.
37. D. Majumdar, D. Dai, and K. Balasubramanian (2000). *J. Chem. Phys.* **113**, 7928.
38. E. Aprà and A. Fortunelli (2003). *J. Phys. Chem. A* **107**, 2934.
39. M. N. Huda, M. K. Niranjan, B. R. Sahu, and L. Kleinman (2006). *Phys. Rev. A* **73**, 053201.
40. T. Jacob, R. P. Muller, and W. A. Goddard (2003). *J. Phys. Chem. B* **107**, 9465.
41. L. Chen, A. C. Cooper, G. P. Pez, and H. S. Cheng (2007). *J. Phys. Chem. C* **111**, 5514.
42. V. Kumar and Y. Kawazoe (2008). *Phys. Rev. B* **77**, 205418.
43. K. Bhattacharyya and C. Majumder (2007). *Chem. Phys. Lett.* **446**, 374.
44. A. Nie, J. Wu, C. Zhou, S. Yao, C. Luo, R. C. Forrey, and H. Cheng (2007). *Int. J. Quantum Chem.* **107**, 219.
45. A. Sebetci and Z. B. Güvenç (2003). *Surf. Sci.* **525**, 66.
46. X. Wang and D. Tian (2009). *Comput. Mater. Sci.* **46**, 239.
47. C. L. Heredia, V. Ferraresi-Curotto, and M. B. Lopez (2012). *Comput. Mater. Sci.* **53**, 18.
48. Z.-Y. Lu, C.-Z. Wang, and K.-M. Ho (2000). *Phys. Rev. B* **61**, 2329.
49. B. Assadollahzadeh, S. Schäfer, and P. Schwerdtfeger (2010). *J. Comput. Chem.* **31**, 929.
50. C. Jo and K. Lee (2000). *J. Chem. Phys.* **113**, 7268.
51. C. Majumder, V. Kumar, H. Mizuseki, and Y. Kawazoe (2001). *Phys. Rev. B* **64**, 233405.

52. F.-c. Chuang, C. Z. Wang, S. Öğüt, J. R. Chelikowsky, and K. M. Ho (2004). *Phys. Rev. B* **69**, 165408.
53. E. Oger, R. Kelting, P. Weis, A. Lechtken, D. Schooss, N. R. M. Crawford, R. Ahlrichs, and M. M. Kappes (2009). *J. Chem. Phys.* **130**, 124305.
54. S. Schäfer, B. Assadollahzadeh, M. Mehring, P. Schwerdtfeger, and R. Schäfer (2008). *J. Phys. Chem. A* **112**, 12312.
55. C. Majumder, V. Kumar, H. Mizuseki, and Y. Kawazoe (2005). *Phys. Rev. B* **71**, 035401.
56. R. Ferrando, A. Fortunelli, and R. L. Johnston (2008). *Phys. Chem. Chem. Phys.* **10**, 640.
57. L. Sai, J. Zhao, X. Huang, and J. Wang (2012). *J. Nanosci. Nanotechnol.* **12**, 132.
58. X. Huang, L. Sai, X. Jiang, and J. Zhao (2013). *Eur. Phys. J. D* **67**, 43.
59. L. Sai, L. Tang, J. Zhao, J. Wang, and V. Kumar (2011). *J. Chem. Phys.* **135**, 184305.
60. L. Sai, L. Tang, X. Huang, G. Chen, J. Zhao, and J. Wang (2012). *Chem. Phys. Lett.* **544**, 7.
61. L. Hong, H. Wang, J. Cheng, X. Huang, L. Sai, and J. Zhao (2012). *Comput. Theor. Chem.* **993**, 36.
62. Z. Jijun and X. Rui-Hua (2004). *J. Comput. Theor. Nanosci.* **1**, 117.
63. J. Ho, M. L. Polak, K. M. Ervin, and W. C. Lineberger (1993). *J. Chem. Phys.* **99**, 8542.
64. M. B. Airola and M. D. Morse (2002). *J. Chem. Phys.* **116**, 1313.
65. J. Donohue *The Structures of the Elements* (Wiley, New York, 1974).
66. J. Ho, M. L. Polak, and W. C. Lineberger (1992). *J. Chem. Phys.* **96**, 144.
67. G. Kresse and J. Furthmüller (1996). *Phys. Rev. B* **54**, 11169.
68. D. W. Smith *Inorganic Substances: A Prelude to the Study of Descriptive Inorganic Chemistry* (Cambridge University Press, Cambridge, 1990).
69. I. Mayer (1986). *Int. J. Quantum Chem.* **29**, 477.